

Spin-lozenge thermodynamics and magnetic excitations in Na_3RuO_4

J. T. Haraldsen^{1,4}, M. B. Stone², M. D. Lumsden², E. Mamontov²,

T. Barnes^{1,3}, R. Jin⁴, J. W. Taylor⁵, and F. Fernandez-Alonso⁵

¹*Department of Physics and Astronomy, University of Tennessee, Knoxville Tennessee 37996, USA*

²*Neutron Scattering Science Division, Oak Ridge National Laboratory, Oak Ridge, Tennessee 37831, USA*

³*Physics Division, Oak Ridge National Laboratory, Oak Ridge, Tennessee 37831, USA*

⁴*Materials Science and Technology Division, Oak Ridge National Laboratory, Oak Ridge, Tennessee 37831, USA and*

⁵*ISIS Facility, Rutherford Appleton Laboratory, Chilton, Didcot, Oxfordshire OX11 0QX, United Kingdom*

(Dated: February 10, 2022)

We report inelastic and elastic neutron scattering, magnetic susceptibility, and heat capacity measurements of polycrystalline sodium ruthenate (Na_3RuO_4). Previous work suggests this material consists of isolated tetramers of $S = 3/2$ Ru^{5+} ions in a so-called “lozenge” configuration. Using a Heisenberg antiferromagnet Hamiltonian, we analytically determine the energy eigenstates for general spin S . From this model, the neutron scattering cross-sections for excitations associated with spin-3/2 spin-tetramer configurations is determined. Comparison of magnetic susceptibility and inelastic neutron scattering results shows that the proposed “lozenge” model is not distinctly supported, but provides evidence that the system may be better described as a pair of non-interacting inequivalent dimers, *i.e.* double dimers. However, the existence of long-range magnetic order below $T_c \approx 28$ K immediately questions such a description. Although no evidence of the lozenge model is observed, future studies on single crystals may further clarify the appropriate magnetic Hamiltonian.

I. INTRODUCTION

Magnetic materials have received continuous research interest since the initial description of the Heisenberg Hamiltonian^{1,2,3,4}. This is due to interest in both the possible technological impact⁵, as well as, fundamental physical phenomenon that many such materials display⁶. Perovskite-based alkali metal ruthenates have just recently started gaining attention^{7,8,9,10}. The ruthenates exhibit a range of properties from ferro- and paramagnetism to superconductivity^{11,12,13}, and have been shown to demonstrate an interesting cross-road in condensed matter physics^{14,15,16,17}. The Na-Ru-O system has sparked interest into the many different analogs which present various magnetic properties from short magnetic order to paramagnetic behavior.¹⁰ Na_3RuO_4 is one such analog that has induced similar queries over its magnetic structure.

The structure of Na_3RuO_4 was first examined by Darriet *et al.*¹⁸. The refinement of the crystal structure in these preliminary measurements show that Na_3RuO_4 consists of oxygen coordinated sodium and ruthenium sites within the *ab* plane, separated by a single layer of sodium sites displaced along the *c*-axis. The structure of Na_3RuO_4 was recently re-refined and was determined to be mono-clinic, with space group $C2/m$ and lattice parameters $a = 11.0295(6)$ Å, $b = 12.8205(7)$ Å, $c = 5.7028(3)$ Å, and $\beta = 109.90(3)^\circ$ ^{10,19}. Figure 1(a) illustrates a single plane of Ru ions together with coplanar oxygen and sodium ions. The Ru ions are octahedrally coordinated through shared oxygens, and each Ru^{5+} ion may be modeled as having a local spin $S = \frac{3}{2}$. This arrangement of ions suggest a local tetramer or lozenge spin system as shown in Fig. 1(a)-(b). An isolated spin-lozenge with exchange constants $J = 3.36$ meV and

$\alpha J = 3.88$ meV was first proposed by Drillon *et al.* in order to describe magnetic susceptibility measurements on this material²⁰. However, the existence of long range antiferromagnetic order below $T \approx 30$ K was established using Mossbauer spectroscopy²¹, and provided the first indication that the suggestion of antiferromagnetic tetramer clusters in Na_3RuO_4 may be incorrect. Recent measurements of magnetic susceptibility have also been interpreted in terms of a spin-tetramer model¹⁰. Temperature dependent neutron diffraction studies have confirmed the existence of long-range magnetic order below $T \approx 30$ K. This long-range order immediately calls into question the accuracy of an isolated spin tetramer model of Na_3RuO_4 .

In the following sections, we present the exact analytical solutions for the energy eigenstates of a general Heisenberg spin S tetramer, and then apply these calculations to the case of spin-3/2 to determine the exact zero-field magnetic susceptibility and inelastic neutron scattering intensities. Through an examination of thermodynamic and spectroscopic properties of Na_3RuO_4 and a comparison with theoretical predictions for various isolated spin tetramers, we shall see that the isolated tetramer model is indeed inappropriate for Na_3RuO_4 .

II. SPIN-S COUPLED DIMER MODEL

Figure 1(b)-(d) shows the individual configurations of the coupled dimer models we examined. As discussed above, Na_3RuO_4 is suggested to consist of isolated Ru^{5+} (spin-3/2) tetramer clusters, where the tetramers are in a lozenge configuration. This is illustrated in Fig. 1(b). In this case, four Ru^{5+} ions have super-exchange interactions through Ru-O-Ru bonds, where the bond lengths

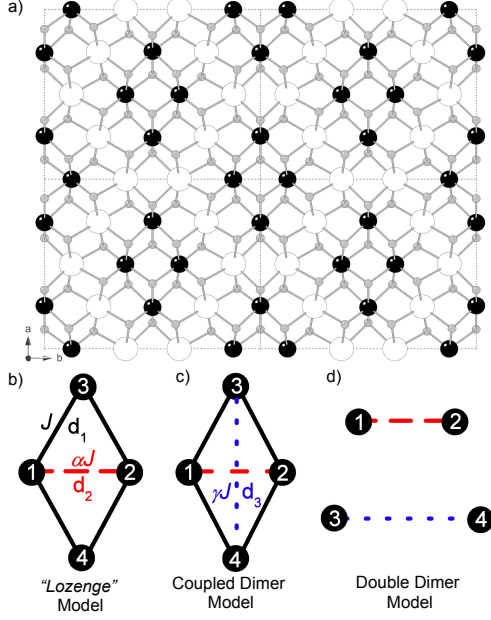


FIG. 1: Crystal structure and potential exchange interactions for Na₃RuO₄. (a) Crystal structure as viewed along the *c*-axis showing a single plane of atomic sites for $\pm \frac{a}{4}$ unit cells. Ru, O and Na sites are black, gray, and white respectively. The monoclinic *C* 2/*m* unit cell is shown as dashed grey lines. (b)-(d) are three possible models of exchange interactions between Ru sites in the *ab* plane as discussed in the text. The double dimer model is not spatially confined, and represents two individual dimers.

were determined by neutron diffraction and are given as 3.20, 3.20 and 5.56 Å for distances d_1 , d_2 , and d_3 , respectively, as illustrated in Fig. 1¹⁰. A more general case of the spin-lozenge model includes a non-zero exchange interaction γJ resulting in the coupled dimer configuration, Fig. 1(c). If $J = 0$, one recovers two isolated dimers or a double dimer configuration, *c.f.* Fig. 1(d). We note that the double dimer model is not spatially confined to the four Ru⁵⁺ ions in the lozenge configuration, but could also represent other dimer interactions in the Na₃RuO₄ crystal structure. Using the coupled dimer model Hamiltonian, we determine the eigenstates for general S , and calculate the corresponding magnetic susceptibility for fitting purposes. Then, with the choice of the appropriate magnetic ground state, the excitations observed with inelastic neutron scattering (INS) and their corresponding structure factors are also determined.

A. Hamiltonian and Energy Eigenstates

All three of the dimer configurations in Fig. 1 can be described by a single Hamiltonian, Eq. 1. By using this

model, we can clearly examine the three possible configurations that may describe Na₃RuO₄. Using nearest-neighbor Heisenberg interactions and a Zeeman magnetic field term for magnetic fields \mathbf{B} defining the *z*-axis, the general Hamiltonian is

$$\mathcal{H} = J \left[(\vec{S}_1 \cdot \vec{S}_3 + \vec{S}_1 \cdot \vec{S}_4 + \vec{S}_2 \cdot \vec{S}_3 + \vec{S}_2 \cdot \vec{S}_4) + \alpha \vec{S}_1 \cdot \vec{S}_2 + \gamma \vec{S}_3 \cdot \vec{S}_4 \right] - (S_1^z + S_2^z + S_3^z + S_4^z) g \mu_B B, \quad (1)$$

where αJ is the interaction for the α -dimer, γJ is the interaction for the γ -dimer, and μ_B is the Bohr magneton. We define the exchange interaction as positive for anti-ferromagnetic interactions, and \vec{S}_i is the quantum spin operator for a spin- S ion at site $i=1,2,3,4$. The Zeeman term interacts with the *z*-component of the spin Hamiltonian, lifting the degeneracy of magnetic substates in applied magnetic fields.

The Hamiltonian, Eq. 1, is rotationally invariant in spin space, such that the total spin, S_{tot} , and S_z are good quantum numbers. For the general case of a spin- S tetramer cluster, the energy eigenstates have the total spin decompositions given by

$$\prod_{S_{tot}=1}^4 S_n = \sum_{S_{tot}=0}^{2S} (4S - S_{tot}) \binom{(S_{tot}+1)(S_{tot}+2)}{2} \oplus \sum_{S_{tot}=0}^{2S-1} S_{tot}^{\frac{1}{2}(4S+2+8S_{tot}S+S_{tot}-3S_{tot}^2)}, \quad (2)$$

where the total number of magnetic states in a general S tetramer are $(2S+1)^4$. Therefore for the $S = 3/2$ tetramer, the energy eigenstates have $S^4 = 256$ magnetic states and the spin decomposition is given by

$$\begin{aligned} & \frac{3}{2} \otimes \frac{3}{2} \otimes \frac{3}{2} \otimes \frac{3}{2} = \\ & \text{Individual Spins,} \\ & (3 \oplus 2 \oplus 1 \oplus 0) \otimes (3 \oplus 2 \oplus 1 \oplus 0) = \\ & \text{Dimer States, and} \\ & 6 \oplus 5^3 \oplus 4^6 \oplus 3^{10} \oplus 2^{11} \oplus 1^9 \oplus 0^4 \\ & \text{Tetramer States.} \end{aligned} \quad (3)$$

The superscript in the tetramer states denote multiple S_{tot} states. Each multiplet containing $2S_{tot}+1$ magnetic states, which are degenerate given an isotropic magnetic Hamiltonian such as the Heisenberg form of Eq. 1, where the degenerate states can be split by a magnetic field. This breakdown of the dimer and tetramer spin states helps clarify which dimer states are interacting to create the composite tetramer states.

By expanding the Kambe approach^{2,22}, we can rewrite the Hamiltonian in terms of total spin for the individual diagonalizable components, in which the eigenstates and eigenvalues of the Hamiltonian may be found by diagonalization in the convenient basis of two dimers. This approach gives information about the states of the dimers as the tetramer states are determined, which allows a clearer picture of the magnetic excitations. In practice,

we employ the usual set of \hat{z} -polarized magnetic basis states. The energy levels are then determined simply by considering a dimer basis, where S_α corresponds to the spin state of the α dimer and S_γ corresponds to the spin state of a γ dimer as described in the Hamiltonian, Eq. 1. Using this dimer basis, the energy levels for the general S coupled dimer can be determined exactly and are given by

$$E = \frac{J}{2} [\mathcal{S}_{tot} + \mathcal{S}_\alpha(\alpha - 1) + \mathcal{S}_\gamma(\gamma - 1) - 2(\alpha + \gamma)\mathcal{S}] \quad (4)$$

where $\mathcal{S}_{tot} = S_{tot}(S_{tot} + 1)$ with S_{tot} denoting the magnetic state of the system, $\mathcal{S}_\alpha = S_\alpha(S_\alpha + 1)$ and S_α is the spin state of the α dimer (S_1 - S_2 dimer), $\mathcal{S}_\gamma = S_\gamma(S_\gamma + 1)$ and S_γ is the spin state of the γ dimer (S_3 - S_4 dimer), and $\mathcal{S} = S(S + 1)$ with S being the spin of the system.

For the $S = \frac{3}{2}$ tetramer, the energy eigenstates of the isotropic Heisenberg Hamiltonian with general S_{tot}^z are given in Table I. The magnetic substates are all degenerate in the absence of an applied magnetic field, but can be split linearly in accordance with the Zeeman field term. The individual states can be split into $2S_{tot} + 1$ states with magnetic field. Therefore, the energy levels split by $g\mu_B B S_{tot}^z$, where S_{tot}^z is from $0 \dots (2S_{tot} + 1)$. The ground state of the $S = \frac{3}{2}$ tetramer can either have a nonmagnetic $S = 0$ ground state or a magnetic $S = 1$ ground state depending upon the values of α and γ . Simple examination of the energy levels in Table I indicates that, assuming antiferromagnetic exchange for J , the ground state will be non-magnetic when both α and γ are less than $\frac{4}{3}$.

B. Spin- $\frac{3}{2}$ Magnetic Observables

Magnetic observables, *i.e.* specific heat and magnetic susceptibility, associated with the general coupled dimer model can be derived via the partition function and eigenvalues. Thus, such macroscopic measurements of Na_3RuO_4 may serve to place limits on the nature of the interactions. We also determine the excitation energies and structure factors which would be observed in INS measurements. Both thermodynamic and spectroscopic measurements should be consistent for any appropriate description of the experimental system.

1. Magnetic Susceptibility and Heat Capacity

We now present the method for determining the partition function and magnetic susceptibility for the $S = 3/2$ coupled dimer model. Due to the length of the equations, we present the eigenstates and eigenvalues explicitly in Table I and represent the magnetic observables as summations over energy eigenvalues. Using this method, the

TABLE I: Energy levels for a spin- $\frac{3}{2}$ lozenge

S_{tot}	Spin State ^a		Energy Level ^b
	$ S_{tot}^z >$	S_α, S_γ	
6	$ 6 S_{tot}^z >$	$3,3$	$J(9 + \frac{9}{4}\alpha + \frac{9}{4}\gamma)$
5	$ 5 S_{tot}^z >$	$3,3$	$J(3 + \frac{9}{4}\alpha + \frac{9}{4}\gamma)$
	$ 5 S_{tot}^z >$	$3,2$	$J(6 + \frac{9}{4}\alpha - \frac{3}{4}\gamma)$
	$ 5 S_{tot}^z >$	$2,3$	$J(6 - \frac{3}{4}\alpha + \frac{9}{4}\gamma)$
4	$ 4 S_{tot}^z >$	$3,3$	$J(-2 + \frac{9}{4}\alpha + \frac{9}{4}\gamma)$
	$ 4 S_{tot}^z >$	$3,2$	$J(1 + \frac{9}{4}\alpha - \frac{3}{4}\gamma)$
	$ 4 S_{tot}^z >$	$3,1$	$J(3 + \frac{9}{4}\alpha - \frac{11}{4}\gamma)$
	$ 4 S_{tot}^z >$	$2,3$	$J(1 - \frac{3}{4}\alpha + \frac{9}{4}\gamma)$
	$ 4 S_{tot}^z >$	$1,3$	$J(3 - \frac{11}{4}\alpha + \frac{9}{4}\gamma)$
	$ 4 S_{tot}^z >$	$2,2$	$J(4 - \frac{3}{4}\alpha - \frac{3}{4}\gamma)$
3	$ 3 S_{tot}^z >$	$3,3$	$J(-6 + \frac{9}{4}\alpha + \frac{9}{4}\gamma)$
	$ 3 S_{tot}^z >$	$3,2$	$J(-3 + \frac{9}{4}\alpha - \frac{3}{4}\gamma)$
	$ 3 S_{tot}^z >$	$3,1$	$J(-1 + \frac{9}{4}\alpha - \frac{11}{4}\gamma)$
	$ 3 S_{tot}^z >$	$2,3$	$J(-3 - \frac{3}{4}\alpha + \frac{9}{4}\gamma)$
	$ 3 S_{tot}^z >$	$1,3$	$J(-1 - \frac{11}{4}\alpha + \frac{9}{4}\gamma)$
	$ 3 S_{tot}^z >$	$2,2$	$J(-\frac{3}{4}\alpha - \frac{3}{4}\gamma)$
	$ 3 S_{tot}^z >$	$2,1$	$J(2 - \frac{3}{4}\alpha - \frac{11}{4}\gamma)$
	$ 3 S_{tot}^z >$	$1,2$	$J(2 - \frac{11}{4}\alpha - \frac{3}{4}\gamma)$
	$ 3 S_{tot}^z >$	$3,0$	$J(\frac{9}{4}\alpha - \frac{15}{4}\gamma)$
	$ 3 S_{tot}^z >$	$0,3$	$J(-\frac{15}{4}\alpha + \frac{9}{4}\gamma)$
2	$ 2 S_{tot}^z >$	$3,3$	$J(-9 + \frac{9}{4}\alpha + \frac{9}{4}\gamma)$
	$ 2 S_{tot}^z >$	$3,2$	$J(-6 + \frac{9}{4}\alpha - \frac{3}{4}\gamma)$
	$ 2 S_{tot}^z >$	$3,1$	$J(-4 + \frac{9}{4}\alpha - \frac{11}{4}\gamma)$
	$ 2 S_{tot}^z >$	$2,3$	$J(-6 - \frac{3}{4}\alpha + \frac{9}{4}\gamma)$
	$ 2 S_{tot}^z >$	$1,3$	$J(-4 - \frac{11}{4}\alpha + \frac{9}{4}\gamma)$
	$ 2 S_{tot}^z >$	$2,2$	$J(-3 - \frac{3}{4}\alpha - \frac{3}{4}\gamma)$
	$ 2 S_{tot}^z >$	$2,1$	$J(-1 - \frac{3}{4}\alpha - \frac{11}{4}\gamma)$
	$ 2 S_{tot}^z >$	$1,2$	$J(-1 - \frac{11}{4}\alpha - \frac{3}{4}\gamma)$
	$ 2 S_{tot}^z >$	$1,1$	$J(1 - \frac{11}{4}\alpha - \frac{11}{4}\gamma)$
	$ 2 S_{tot}^z >$	$2,0$	$J(-\frac{3}{4}\alpha - \frac{15}{4}\gamma)$
	$ 2 S_{tot}^z >$	$0,2$	$J(-\frac{15}{4}\alpha - \frac{3}{4}\gamma)$
1	$ 1 S_{tot}^z >$	$3,3$	$J(-11 + \frac{9}{4}\alpha + \frac{9}{4}\gamma)$
	$ 1 S_{tot}^z >$	$3,2$	$J(-8 + \frac{9}{4}\alpha - \frac{3}{4}\gamma)$
	$ 1 S_{tot}^z >$	$2,3$	$J(-8 - \frac{3}{4}\alpha + \frac{9}{4}\gamma)$
	$ 1 S_{tot}^z >$	$2,2$	$J(-5 - \frac{3}{4}\alpha - \frac{11}{4}\gamma)$
	$ 1 S_{tot}^z >$	$2,1$	$J(-3 - \frac{3}{4}\alpha - \frac{11}{4}\gamma)$
	$ 1 S_{tot}^z >$	$1,2$	$J(-3 - \frac{11}{4}\alpha - \frac{3}{4}\gamma)$
	$ 1 S_{tot}^z >$	$1,1$	$J(-1 - \frac{11}{4}\alpha - \frac{11}{4}\gamma)$
	$ 1 S_{tot}^z >$	$1,0$	$J(-\frac{11}{4}\alpha - \frac{15}{4}\gamma)$
	$ 1 S_{tot}^z >$	$0,1$	$J(-\frac{15}{4}\alpha - \frac{11}{4}\gamma)$
0	$ 0 S_{tot}^z >$	$3,3$	$J(-12 + \frac{9}{4}\alpha + \frac{9}{4}\gamma)$
	$ 0 S_{tot}^z >$	$2,2$	$J(-6 - \frac{3}{4}\alpha - \frac{3}{4}\gamma)$
	$ 0 S_{tot}^z >$	$1,1$	$J(-2 - \frac{11}{4}\alpha - \frac{11}{4}\gamma)$
	$ 0 S_{tot}^z >$	$0,0$	$J(-\frac{15}{4}\alpha - \frac{15}{4}\gamma)$

^a S_α and S_γ are the spin state of the α and γ dimers.

^bThe magnetic field splitting of the states is given by the addition of a $S_{tot}^z g\mu_B B$ to the energy of the magnetic states.

canonical partition function is given by

$$Z = \sum_{i=1}^N e^{-\beta E_i} = \sum_{E_i} (2S_{tot} + 1) e^{-\beta E_i} \quad (5)$$

and the magnetic susceptibility is given by

$$\begin{aligned} \chi &= \frac{\beta}{Z} \sum_{i=1}^N (M_z^2)_i e^{-\beta E_i} \\ &= \frac{1}{3} (g\mu_B)^2 \frac{\beta}{Z} \sum_{E_i} (2S_{tot} + 1) (S_{tot} + 1) S_{tot} e^{-\beta E_i} . \end{aligned} \quad (6)$$

In these formulas, the sum $\sum_{i=1}^N$ is over all N independent energy eigenstates (including magnetic substates), the sum \sum_{E_i} is over energy levels only, $M_z = mg\mu_B$ where $m = S_{tot}^z/\hbar$ is the integral or half-integral magnetic quantum number, g is the Lande g -factor, $\beta = \frac{1}{k_B T}$ and k_B is Boltzmann's constant⁴. The heat capacity can also be determined from

$$C = k_B \beta^2 \frac{d^2 \ln(Z)}{d\beta^2} . \quad (7)$$

In general, the heat capacity is especially useful for confirming the proper accounting of eigenstates through a numerical calculation of the magnetic entropy of the tetramer system at large temperature,

$$\begin{aligned} \frac{S}{k_B} &= \int_0^\infty \frac{C}{k_B} \frac{d\beta}{\beta} = \\ \ln(\mathcal{N}/\mathcal{N}_0) &= \begin{cases} 2 \ln(2), & \alpha < \frac{4}{3} \text{ and } \gamma < \frac{4}{3} \\ \ln(\frac{256}{3}), & \alpha > \frac{4}{3} \text{ or } \gamma > \frac{4}{3}. \end{cases} \end{aligned} \quad (8)$$

Here \mathcal{N} is the dimensionality of the full Hilbert space and \mathcal{N}_0 is the degeneracy of the ground state manifold. The numerical calculation of entropy within various regions of α and γ confirms the ground state of the spin-3/2 tetramer.

2. Inelastic Neutron Scattering

The experimental focus of this paper is the use of INS to investigate the nature of the magnetic interactions and their respective excitations. Using methods presented in Haraldsen *et al.*^{23,24}, we next determine the excitation energies and structure factors for the observable transitions of the coupled dimer models shown in Figs. 1(b)-(d).

For transitions out of the ground state, the excitation energy, $\hbar\omega$, is simply the difference in energy between the excited and ground states. Such excitations would be non-dispersive in the absence of inter-tetramer exchange. The differential cross-section of finite systems is proportional to the neutron scattering structure factor

$$S(\vec{q}) = |\mathbf{F}(\vec{q})|^2 \left[\sum_{\lambda_f} \langle \Psi_f(\lambda_f) | V_a | \Psi_i \rangle^2 \right] \quad (9)$$

where $\mathbf{F}(\vec{q})$ is the magnetic form factor and the vector $V_a(\vec{q})$ is a sum of spin operators over all magnetic ions in a unit cell

$$V_a = \sum_{\vec{x}_i} S_a(\vec{x}_i) e^{i\vec{q} \cdot \vec{x}_i} . \quad (10)$$

For rotationally invariant magnetic interactions and an $S_{tot} = 0$ ground state in the $T = 0$ limit, only $S_{tot} = 1$ final states as shown in Table I are observable via INS. However, due to the nature of the tetramer states as being composite dimer states, this implies that it is only possible to excite transitions of the individual dimers which make up the tetramer structure, $\Delta S_{\alpha/\gamma} = \pm 1, 0$. To interpret neutron experiments on powder samples, we require an orientation average of the unpolarized single-crystal neutron scattering structure factor. We define this powder average by

$$\bar{S}(q) = \int \frac{d\Omega_{\hat{q}}}{4\pi} S(\vec{q}) . \quad (11)$$

With respect to the spin-3/2 rhombus model, the values of the magnetic interactions quoted in the literature suggest a $S_{tot} = 0$ ground state, with dimer spins $S_\alpha = 3$ and $S_\gamma = 3$ ^{10,20}. Therefore, due to this selective restriction of the spin excitations, only three of the nine $S_{tot} = 1$ states are accessible from that ground state through INS. The respective excitation energies ($E_{S_{tot}, S_\alpha, S_\gamma}$) are

$$\begin{aligned} E_{0,3,3 \rightarrow 1,3,3} &= J, \\ E_{0,3,3 \rightarrow 1,3,2} &= J(4 - 3\gamma), \\ E_{0,3,3 \rightarrow 1,2,3} &= J(4 - 3\alpha), \end{aligned} \quad (12)$$

and the powder average INS structure factors ($\bar{S}(q)_{S_{tot}, S_\alpha, S_\gamma}$) for these transitions are

$$\begin{aligned} \bar{S}(q)_{0,3,3 \rightarrow 1,3,3} &= 2|\mathbf{F}(\vec{q})|^2 (2 - 4j_0(qd_1) + j_0(qd_2) + j_0(qd_3)), \\ \bar{S}(q)_{0,3,3 \rightarrow 1,3,2} &= \frac{|\mathbf{F}(\vec{q})|^2}{2} (1 - j_0(qd_3)), \\ \bar{S}(q)_{0,3,3 \rightarrow 1,2,3} &= \frac{|\mathbf{F}(\vec{q})|^2}{2} (1 - j_0(qd_2)), \end{aligned} \quad (13)$$

where d_1 , d_2 , and d_3 are the interatomic separations (shown in Fig. 1), $j_0(x) = \frac{\sin(x)}{x}$, and $|\mathbf{F}(\vec{q})|$ is the Ru^{5+} magnetic form factor (a parameterization is given by Parkinson *et al.*^{25,26}). The transition of $|00 \rangle_{3,3} \rightarrow |1S_{tot}^z \rangle_{3,3}$ is an excitation of the full tetramer, while the other two transitions are excitations of individual dimers. This shows that out of the nine possible spin-1 states to be excited for the spin- $\frac{3}{2}$ model, only three are accessible by INS and will have a corresponding intensity profile. The unseen transitions are inaccessible because they require multiple spin transitions, and since a neutron can only provide one transition, only transitions that excite the individual components will be observed by neutron scattering.

III. EXPERIMENTAL TECHNIQUES

Powder samples of Na_3RuO_4 were prepared by solid-state reactions from stoichiometric amount of NaOH and RuO_2 . The starting stoichiometric mixture was initially ground together and then held at 500°C for 20 hr. under an O_2 atmosphere. After re-grinding, the powder was heated to 650°C for another 20 hr, again under an O_2 atmosphere. The resulting dark grey powder was reground and checked for impurity phases using X-ray powder diffraction. If any impurity phases were evident, the powder was refired and the process repeated. This growth procedure is similar to that described in Ref. 10. Powder refinement of room temperature X-ray diffraction measurements yielded lattice parameters of $a = 11.012(7)$, $b = 12.809(9)$, $c = 5.687(3)$ Å, and $\beta = 109.91(3)^\circ$ for the $C2/m$ monoclinic unit cell¹⁹. These values compare well to the fully refined structure described in Ref. 10. Single crystals of appropriate mass are unfortunately not yet available for INS measurements.

Heat capacity measurements were performed on a small single crystal of mass ≈ 10 mg, which was obtained through the synthesis procedure described above. This single crystal grew as a small platelet, with the c -axis normal to the plane of the platelet. Heat capacity measurements were performed with a commercial calorimeter between $T = 1.8$ K and 300 K, using the relaxation technique. Measurements were carried out in zero and 8 T applied magnetic fields, with the field applied along the c -axis of the single crystal sample.

Magnetization measurements were performed on powder and single crystal samples using a commercial SQUID, as a function of applied magnetic field and temperature. SQUID measurements on the same single crystal sample that was used for heat capacity measurements agree well with those taken on a powder sample.

INS measurements were performed using the MARI time-of-flight spectrometer at the ISIS neutron scattering facility²⁷. The sample consisted of ≈ 45 g of Na_3RuO_4 powder in a square aluminum foil sachet (approximately 50 by 50 by 8 mm), suspended from the cold-tip of a closed-cycle He^4 refrigerator. The sachet was oriented with the 50x50 mm surface normal to the incident neutron beam. An incident energy of $E_i = 25$ meV was used, and data were taken at several temperatures between $T = 8$ K and $T = 305$ K. This configuration resulted in a measured instrumental energy resolution at the elastic position of $\delta\hbar\omega = 0.982(7)$ meV full width at half maximum (FWHM). Data were corrected for detector sensitivity through room temperature measurements on a vanadium standard.

INS measurements were also carried out using the HB3 triple-axis spectrometer at the high flux isotope reactor (HFIR) at Oak Ridge National Laboratory. For these measurements, the sample consisted of 20.7 g of Na_3RuO_4 powder in a cylindrical aluminum sample can of 18 mm diameter and 57 mm height. The sample can was sealed under He gas and mounted to the cold-tip

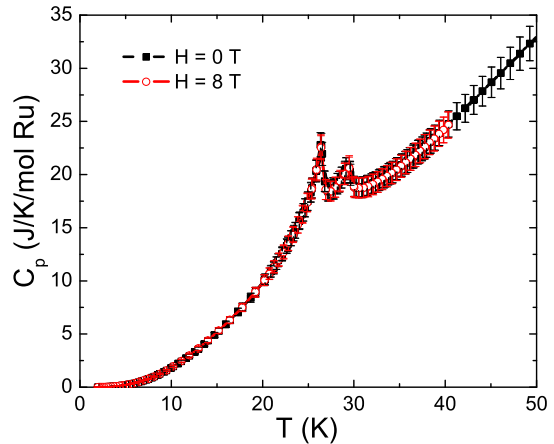


FIG. 2: Heat capacity of a Na_3RuO_4 single crystal. Measurements were performed at zero field (black squares) and $H = 8$ T (red open circles), with $H \parallel c$. Error bars represent an estimated five percent error in the measurement.

of a closed-cycle He^4 refrigerator. Horizontal collimation was chosen as $48' - 40' - 40' - 120'$ between source and monochromator, monochromator and sample, sample and analyzer, and analyzer and detector, respectively. The spectrometer was operated with fixed final energy, $E_f = 14.7$ meV, using a pyrolytic graphite (PG 002) monochromator and analyzer. Pyrolytic graphite filters were placed after the sample to substantially reduce higher-order spurious scattering processes. In this configuration, the energy resolution at the elastic position was $\delta\hbar\omega = 1.10(2)$ meV FWHM, as measured from the incoherent scattering at $Q = 1.2$ Å⁻¹. The wave vector resolution was measured to be $\delta Q = 0.0407(7)$ Å⁻¹ FWHM using the (110) nuclear Bragg peak. All measurements were made for fixed incident neutron monitor count.

Elastic neutron scattering measurements were also performed using the HB3 triple-axis spectrometer, with $E_i = E_f = 14.7$ meV. These measurements were performed on the same powder sample as the inelastic HB3 measurements, with horizontal collimation $48' - 20' - 20' - 70'$. This resulted in an energy resolution at the elastic position of $\delta\hbar\omega \approx 0.8$ meV FWHM. The wave vector resolution was measured to be $\delta Q = 0.0254(9)$ Å⁻¹ FWHM using the (110) nuclear Bragg peak.

INS measurements were also performed to place limits on the value of a possible energy gap in the excitation spectrum. These were performed using the IRIS backscattering spectrometer at the ISIS neutron source at the Rutherford Appleton Laboratory²⁸. The sample measured was the identical powder used for the HB3 measurements. The IRIS spectrometer was operated at 25 Hz with cooled PG002 analyzers ($T = 10$ K) and a Beryllium filter ($T = 25$ K) to avoid contamination from higher-

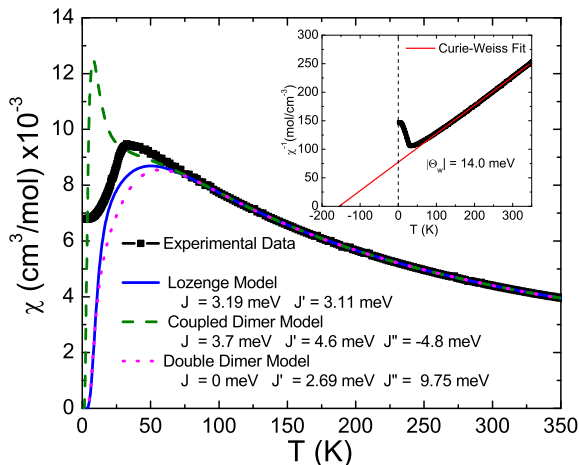


FIG. 3: Magnetic susceptibility of Na_3RuO_4 powder (black squares), showing fits using the three models: Lozenge (solid blue), coupled dimer (dashed green), double dimer (dotted magenta). The inset shows χ^{-1} , with a Curie-Weiss fit as described in the text (which gives $|\Theta_{CW}| = 14.0$ meV, and is consistent with dominantly antiferromagnetic interactions.)

order reflections, resulting in a $17.5 \mu\text{eV}$ FWHM energy resolution at the elastic position as measured with a vanadium standard. The high-resolution (back-scattering) diffraction banks with a resolution of $\frac{\Delta Q}{Q} = 2.5 \text{ E-3}$ were also used on IRIS.

IV. EXPERIMENTAL RESULTS

Figure 2 shows the heat capacity as a function of temperature for $H = 0$ and 8 T. There are two clear lambda-like anomalies at $T \approx 23$ and $T \approx 28$ K, signifying phase transitions at these temperatures. Previous neutron diffraction measurements have shown the existence of only a single, broad phase transition near 30 K in Na_3RuO_4 , corresponding to the onset of long-range magnetic order¹⁰. Our heat capacity measurements indicate that the observed broad transition is likely due to two successive transitions that occur at similar temperatures. No change was noted in these transition temperatures when measured at $H = 0$ and $H = 8$ T.

The magnetic susceptibility of Na_3RuO_4 was measured over the range $2 \leq T \leq 350$ K; the resulting data is shown in Fig. 3. The susceptibility also shows evidence for a phase transition near $T \approx 30$ K. The negative intercept in $\chi^{-1}(T)$ and the decrease in $\chi(T)$ below the transition temperature are consistent with dominantly antiferromagnetic interactions.

Figure 4 shows the temperature dependent inelastic

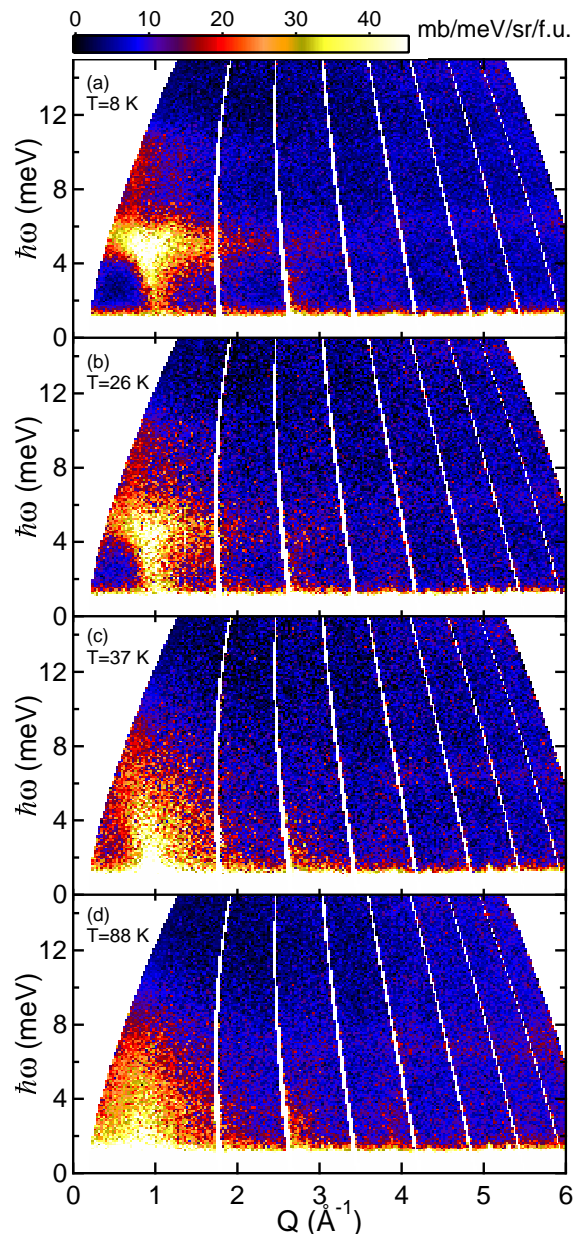


FIG. 4: INS intensity from Na_3RuO_4 powder versus energy and momentum transfer at (a) $T = 8$ K, (b) $T = 26$ K, (c) $T = 37$ K and (d) $T = 88$ K. These measurements were carried out on the MARI spectrometer at an incident energy of $E_i = 25$ meV.

neutron scattering data taken on the MARI spectrometer at ISIS. There is significant inelastic scattering intensity in the vicinity of $\hbar\omega \approx 5$ meV, which decreases in intensity rapidly with increasing wave-vector. The wave-vector dependence implies that the scattering is magnetic in origin. In the $T = 8$ K data, a weak excitation near $\hbar\omega \approx 10$ meV is also evident. As the temperature increases, the inelastic scattering intensity rapidly decreases and moves to smaller wave-vectors, consistent with an evolution from antiferromagnetic spin-

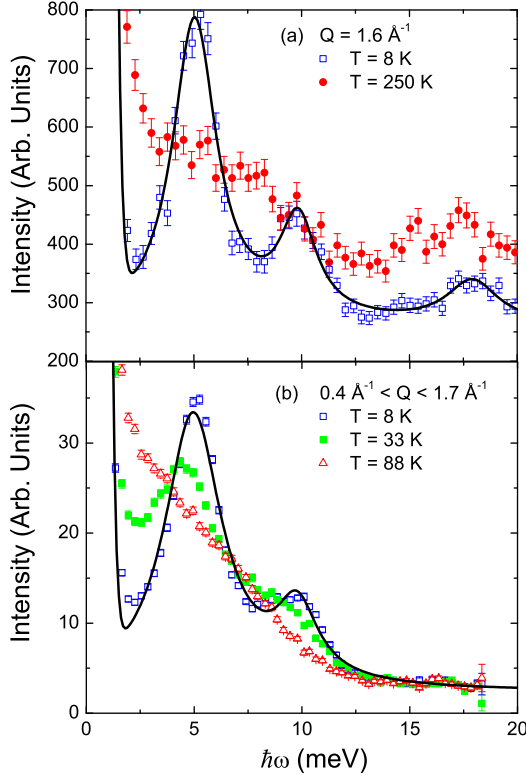


FIG. 5: INS intensity from Na_3RuO_4 powder versus energy transfer at (a) $Q = 1.6 \text{ \AA}^{-1}$ at $T = 8$ and 250 K and (b) integrated between $0.4 \text{ \AA}^{-1} < Q < 1.7 \text{ \AA}^{-1}$ at $T = 8 \text{ K}$, 30 K and 88 K . Black lines are Lorentzian fits, as described in the text. The data in (a) are from HB3, and the data in (b) are from MARI.

waves to paramagnetic scattering with increasing temperature. We speculate that the excitations observed below T_N are acoustic and optical spin-waves associated with the long-range ordered phase. Higher incident energy measurements were also performed, which show evidence for phonon excitations above 20 meV .

In Fig. 5, we show the scattering intensity as a function of energy transfer for the single wave-vector $Q = 1.6 \text{ \AA}^{-1}$, measured on the HB3 spectrometer, as well as the integrated scattering intensity for $0.4 \text{ \AA}^{-1} < Q < 1.7 \text{ \AA}^{-1}$ on the MARI spectrometer. Single Lorentzian fits to the low-temperature data suggest modes at $\hbar\omega = 5.03 \pm 0.08$, 9.8 ± 0.2 and $17.9 \pm 0.3 \text{ meV}$ (for the data shown in Fig. 5(a)), and $\hbar\omega = 4.95 \pm 0.04$ and $9.8 \pm 0.1 \text{ meV}$ for the data shown in Fig. 5(b). The increase in intensity of the 18 meV excitation with increasing temperatures suggests that it is likely a phonon excitation.

The 18 meV phonon excitation was investigated more carefully as a function of temperature and wave-vector, as

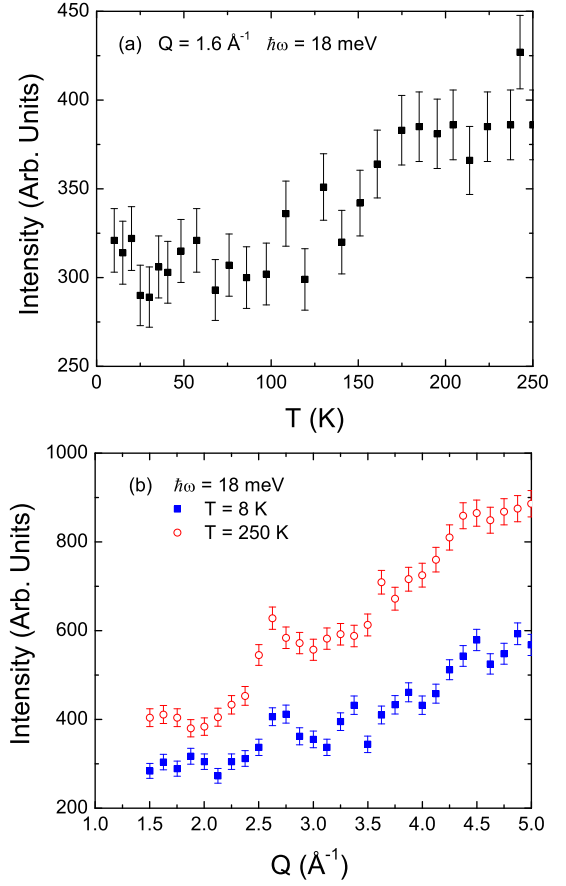


FIG. 6: (a) INS intensity versus temperature at $\hbar\omega = 18 \text{ meV}$ and $Q = 1.6 \text{ \AA}^{-1}$. (b) INS intensity versus momentum transfer at $\hbar\omega = 18 \text{ meV}$ at $T = 8$ and $T = 250 \text{ K}$. Data were acquired using HB3.

shown in Fig. 6. These data show a monotonic increase in scattering intensity as the temperature is increased, and an increase in scattering intensity with increasing wave-vector. These results further support the identification of the 18 meV mode with a phonon excitation.

We also examined the temperature dependence of the elastic scattering in the vicinity of $Q \approx 1 \text{ \AA}^{-1}$. Figure 7 shows the scattering intensity observed in the HB3 Na_3RuO_4 powder measurement as a function of temperature and wave-vector. As the temperature is decreased, there is an increase in the scattering intensity at $Q \approx 0.99$ and $\approx 1.07 \text{ \AA}^{-1}$ corresponding to the transition to long range magnetic ordering. Below $T \approx 25 \text{ K}$, the magnetic Bragg peaks appear to move as a function of decreasing temperature. This is also evident in Fig. 8, which shows the scattering intensity as a function of temperature for various individual momentum transfers. For certain Q values, the scattering intensity shows

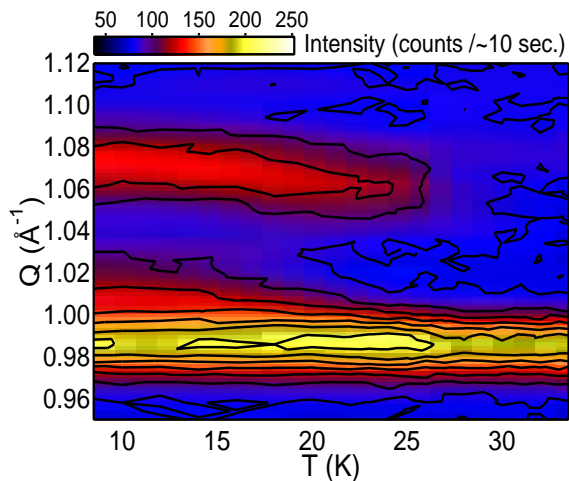


FIG. 7: Elastic scattering intensity of Na_3RuO_4 as function of momentum transfer and temperature. Data were acquired using the HB3 spectrometer. The contour lines correspond to intervals of 20 counts per ten seconds, and are only plotted for count rates between 80 and 200 counts per ten seconds. The data were obtained at 20 temperatures between $T = 8.5$ and 34 K.

non-monotonic temperature dependence, for example as shown in Fig. 7 at $Q = 0.99 \text{ \AA}^{-1}$ and 1.05 \AA^{-1} . These behaviors may be due to the presence of two magnetic phase transitions near 25-30 K as seen in the heat capacity measurements.

High resolution backscattering measurements investigated the magnetic spectrum for energy transfers below 1.7 meV (shown in Fig. 9(a)). Excitations are populated out of the $Q \approx 1.1 \text{ \AA}^{-1}$ wave-vector with a very steep dispersion at such low energy transfers. Figure. 9(b) shows the difference of the elastic scattering intensity between the disordered and ordered phases as measured using IRIS and HB3 illustrating the low-temperature powder magnetic Bragg peaks in Na_3RuO_4 . These data illustrate that the excitations are dispersing directly out of the magnetic Bragg peaks. The data in Figs. 9(a) show no indication of a gap in the magnetic spectrum down to $\sim 250 \text{ \mu eV}$.

V. DISCUSSION

The high temperature magnetic susceptibility fitted using the finite cluster models for $T > 30 \text{ K}$ (where there is no long range order). Table II shows the magnetic interactions determined from these fits for the three models considered. We also compare the extracted magnetic interaction parameters to the Curie-Weiss temperature. The Curie-Weiss temperature in a mean field approximation is

$$\Theta_W = \frac{S(S+1)}{3} J_0, \quad (14)$$

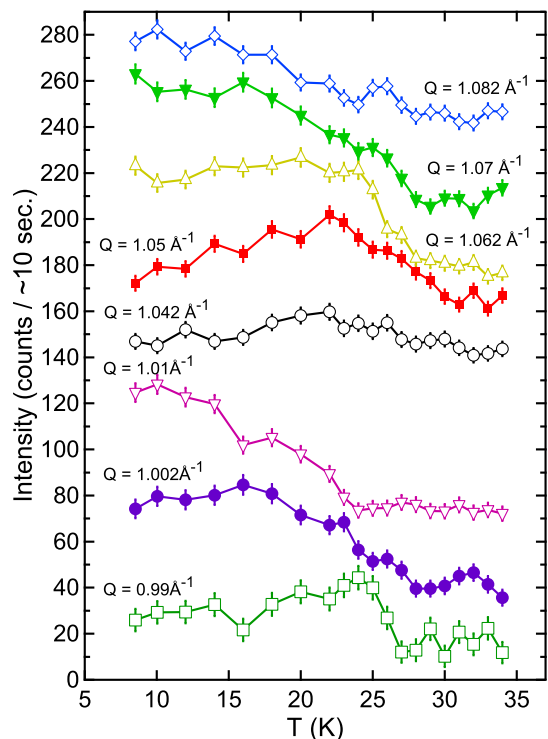


FIG. 8: Elastic scattering intensity from Na_3RuO_4 powder versus temperature for several wave-vectors. The data correspond to the individual wave-vectors shown in Fig. 7. The data have been offset along the vertical axis for presentation.

where, in this case, $S = \frac{3}{2}$ and J_0 is the sum of the magnetic exchange constants²⁹. As shown in Fig. 3, all three cluster models qualitatively reproduce the high temperature susceptibility data, and only deviate strongly close to the transition temperature. However, a comparison of the calculated Curie-Weiss temperatures based upon the double dimer model is more consistent with the experimental Curie-Weiss temperature, $|\Theta_W| = 14.0 \text{ meV}$ (antiferromagnetic), illustrated in the inset of Fig. 3. Because the Curie-Weiss temperature is proportional to a sum of exchange constants, the presence of inter-cluster exchange could significantly effect the estimate value of Θ_W . For example, there are 28 bonds with distances of five to six angstroms between the Ru sites in one cluster and the Ru sites in all neighboring clusters. If inter-cluster interactions are large, the estimated Curie-Weiss temperature would deviate significantly from the values quotes in Table II.

The inelastic neutron scattering energies and intensities can also be calculated using the exchange values determined from the magnetic susceptibility (Table II) and the ion positions given by Regan *et al.*¹⁰ The three models predict INS observable energy gaps of 2.96, 3.08, and 12.16 meV for the lozenge model, 1.33, 3.49, and 23.53 meV for the coupled dimer model, and 2.47 and 9.16 meV for the double dimer model. We have already noted that the data shows magnetic excitations at approximately

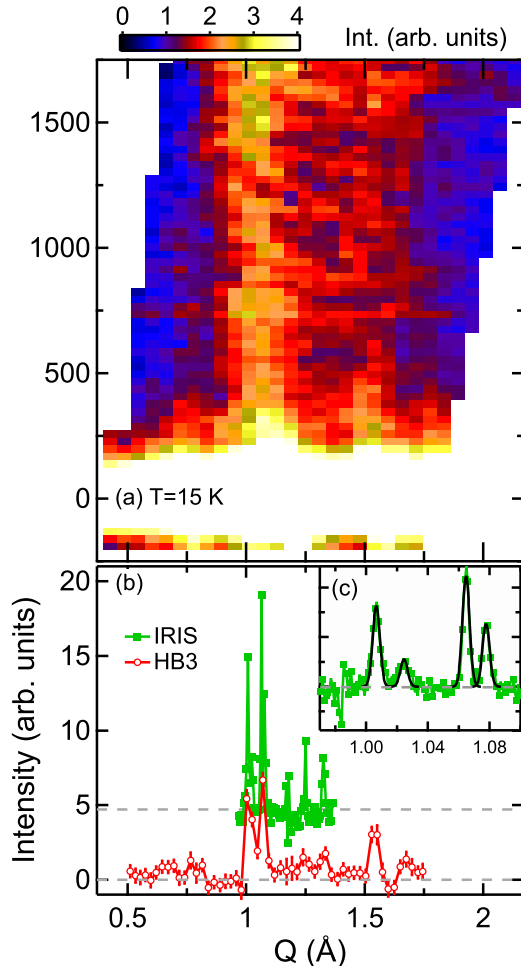


FIG. 9: (a) $T = 15$ K Powder INS scattering intensity from Na_3RuO_4 as a function of energy and wave-vector transfer measured using the IRIS spectrometer at ISIS. (b) Intensity as a function of wave-vector transfer for data acquired at both IRIS and HB3. IRIS data were acquired at $T = 8$ and 30 K using the high resolution diffraction banks. HB3 data were acquired in same configuration as Fig. 7 at $T = 8$ and 30 K. Both data sets indicate clear peaks at 1.0 and 1.07 Å⁻¹. Panel (c) shows the high resolution IRIS data fitted to a series of single width Gaussian peaks at $Q = 1.006(1)$, $1.025(4)$, $1.065(1)$ and $1.078(1)$ Å⁻¹.

5.0 and 9.8 meV, *cf.* Fig. 5. Figures 4 and 9 also show evidence for a spin-wave emerging from the antiferromagnetic Bragg peak in the vicinity of the $Q \approx 1$ Å⁻¹ for $T < T_N$. Although a clear transition to long-range magnetic order is evident at low temperatures, it is nonetheless reasonable to examine the properties of these excitations as observed in INS especially their wave-vector dependence, since these are characteristic indicators of the nature of the interactions.

On comparing the predicted excitation spectrum, using the magnetic susceptibility data to determine the interaction strengths, the double dimer model seems to

give the most realistic description of the excitation energies. We note however that the inter-cluster interactions which produce long-range order may significantly affect the energy levels. All three models predict an INS visible excitations below 3 meV and above 9 meV. We also examine the wave-vector dependence of these three models; Figure 10 shows constant energy scans performed above and below T_N at 5.0 and 9.8 meV energy transfer. For comparison, we first calculate the wave-vector dependence of the INS scattering intensity using Eq. 13 for the lozenge model geometry. These lineshapes (shown in Fig. 10) are unable to account for the initial rapid rise in scattering intensity at small wave-vectors, which implies that there are significant exchange interactions between spins at larger separations than are present in the lozenge model. If the ionic distances are allowed to vary freely in fitting the data, an interesting result emerges. For the 9.8 meV excitation, the fitted dimer separation in a single dimer model is 5.66 ± 0.10 Å bond. This separation agrees with the length of the γ -dimer. This makes it unlikely that the coupled dimer model is realistic, as it predicts a 23 meV γ -dimer excitation using the magnetic susceptibility parameter. The lozenge and double-dimer models with susceptibility-fitted parameters predict γ -dimer excitations at 12 meV and 9 meV, respectively. The double dimer model is evidently closer to the observed gap of 9.8 meV. Fitting the 5.0 meV data with a free dimer length in which, both the lozenge and dimer models gives a length of 4.60 ± 0.02 Å, which does not correspond to any Ru-Ru separation in the structure of Na_3RuO_4 . We conclude that the intercluster interactions are important enough to modify the energies and wave-vector dependences of the excitations, so that the three simple dimer models do not give a decent description of the excitations.

In Table II, gives estimated magnetic interaction parameters for the various models using the observed neutron scattering excitations at $\hbar\omega \approx 5.03$ and 9.8 meV as input. Since no third magnetic excitation was observed to 30 meV, the coupled dimer model cannot be uniquely constrained. Although the lozenge model also predicts three excitations, two of those excitations involve dimers. Therefore, we can determine both exchange constants using the neutron scattering results. Using these exchange interactions, the lozenge model gives an estimated Curie-Weiss temperature of 29.5 meV, more than double the observed value from magnetic susceptibility. The double dimer model gives a value of $|\Theta_w| = 18.5$ meV; this is closer to the measured value, although it is still 30% larger than the observed value (from the magnetic susceptibility). If the excitations are indeed well described by the double dimer model, then they demonstrate that the 5.0 and 9.8 meV modes correspond to excitations of the α - and γ -dimers, with the nature of the α -dimer excitation being significantly modified coupled-cluster effects and the onset of long-range magnetic order.

TABLE II: **Exchange interactions estimated from the magnetic susceptibility and inelastic neutron scattering.**

Curie-Weiss Fit				
$ \Theta_w = 14.0 \pm 0.2$ meV				
Magnetic Susceptibility				
Model	J (meV)	αJ (meV)	γJ (meV)	$ \Theta_w $ (meV)
Lozenge	3.19 ± 0.01	3.11 ± 0.03		19.8 ± 0.1
Coupled Dimer	3.7 ± 0.1	4.6 ± 0.3	-4.8 ± 1.2	18.3 ± 1.3
Double Dimer		2.69 ± 0.01	9.75 ± 0.05	15.6 ± 0.1
Inelastic Neutron Scattering ^a				
Model	J (meV)	αJ (meV)	γJ (meV)	$ \Theta_w $ (meV)
Lozenge	5.03 ± 0.08		3.5 ± 0.1	29.5 ± 0.1
Double Dimer		5.03 ± 0.08	9.8 ± 0.2	18.5 ± 0.1

^aThere is insufficient information to determine the interaction strengths in the coupled dimer model.

VI. CONCLUSIONS

In summary, we have given analytical results for the energy eigenvalues and eigenstates for coupled dimers with general spin S ions. We derive analytical closed-form results for magnetic susceptibility and inelastic neutron scattering excitation functions and their wave-vector dependences for several tetramer models, and compare our results to experimental data on the $S = 3/2$ tetramer spin lozenge candidate, Na_3RuO_4 .

On considering the observed magnetic susceptibility and inelastic neutron scattering data and comparing these results to several tetramer models, we first find that the Na_3RuO_4 data is not consistent with the spin-lozenge model of Regan *et al.*¹⁰. Although no isolated tetramer model is able to describe all of the thermodynamic and spectroscopic measurements simultaneously, a double dimer model, with bond lengths of 4.60 Å and 5.66 Å, does provide a description of some aspects of the observed thermodynamic properties and the inelastic neutron scattering measurements on the two observed magnetic excitations. However, only one spatial distance corresponds to length seen in the material shown in Fig. 1.

Measurements of the heat capacity and elastic neutron scattering data show that there are two distinct magnetic phase transitions in this material, at $T \approx 23$ and 28 K (This is the first evidence for two low-temperature phase transitions in this material). Clearly, an understanding the nature of these long-range ordered magnetic phases will provide useful additional information regarding the nature of magnetic interactions in Na_3RuO_4 . We an-

ticipate that neutron diffraction measurements on single

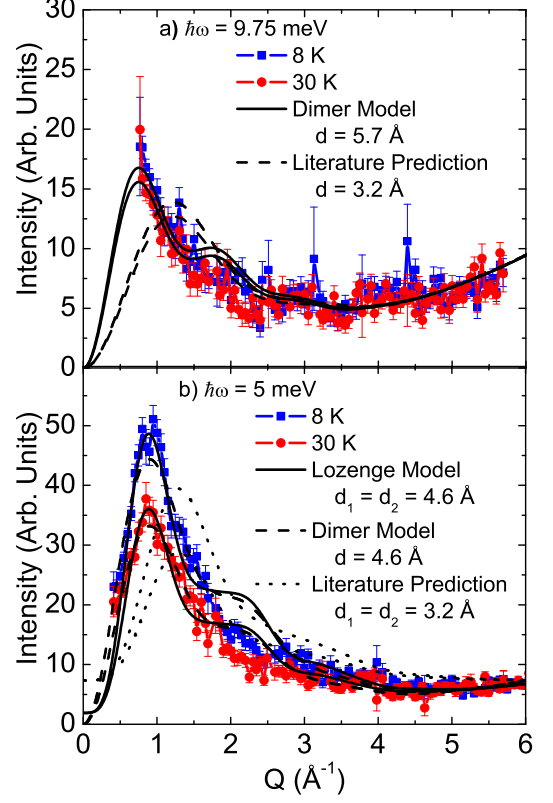


FIG. 10: a) INS intensity versus momentum transfer of the 9.8 meV excitation in Na_3RuO_4 at $T = 8$ K (blue squares) and 30 K (red circles); the black solid lines are fits to the dimer model and the gray dashed lines are predictions given fixed physical distances. b) INS intensity versus momentum transfer at $T = 8$ K (blue squares) and 30 K (red circles) for the 5.0 meV excitation. The solid black line is the lozenge model fit, the dashed gray line is the dimer model fit, and dotted light gray line is a prediction using physical distances (The data were taken using the MARI spectrometer at ISIS, as described in the text).

crystal samples of Na_3RuO_4 will be the most useful next step in the experimental studies of this material.

VII. ACKNOWLEDGMENTS

We would like to acknowledge the Joint Institute for Neutron Sciences for funding and support. We thank S. Nagler for helpful discussions. The research at Oak Ridge National Laboratory was sponsored by the Scientific User Facilities Division, Office of Basic Energy Sciences, U. S. Department of Energy.

-
- ¹ W. Heisenberg, Z. Phys. **38**, 411 (1926)
 - ² D. Gatteschi, R. Sessoli, and J. Villain *Molecular Nanomagnets* (Oxford University Press, 2006).
 - ³ E. Dagotto and T. M. Rice, Science **271**, 618 (1996).
 - ⁴ O.Kahn, *Molecular Magnetism* (VCH Publishers, New York, 1993).
 - ⁵ M. A. Nielsen and I. L. Chuang, *Quantum Computation and Quantum Information* (Cambridge, 2000).
 - ⁶ A. L. Barra, A. Caneschi, A. Cornia, F. Frabrizide de Biani, D. Gatteschi, C. Sangregorio, R. Sessoli, and L. Sorace, J. Am. Chem. Soc. **121**, 5302 (1999).
 - ⁷ I. S. Shaplygin and V. B. Lazarev, Russ. J. Inorg. Chem. **25**, 1837 (1980).
 - ⁸ M. Shikano, C. Delmas, J. Darriet, Inorg. Chem. **43**, 1214 (2004).
 - ⁹ M. Shikano, R. K. Kremer, M. Ahrens, H.-J Koo, M.-H Whangbo, and J. Darriet, Inorg. Chem. **43**, 5 (2004).
 - ¹⁰ K. A. Regan, Q. Huang and R. J. Cava, J. Solid State Chem. **178**, 2104 (2005).
 - ¹¹ A. Callaghan, C. W. Moeller, and R. Ward, Inorg. Chem **5**, 1572 (1966).
 - ¹² J. T. Rijssenbeek, R. Jin, Y. Zadorozhny, Y. Liu, B. Batlogg, and R. J. Cava, Phys. Rev. B **59**, 4561 (1999).
 - ¹³ Y. Maeno, H. Hashimoto, K. Yoshida, S. Hishizaki, T. Fujita, J.G. Bernorz, and F. Lichtenberg, Nature **372**, 532 (1994).
 - ¹⁴ R. J. Cava, J. Chem. Soc. Dalton Trans. **19**, 2979 (2004).
 - ¹⁵ K. A. Regan, Q. Huang, M. Lee, A.P. Ramirez, and R.J. Cava, J. Solid State Chem. **179**, 195 (2006).
 - ¹⁶ A. Alexander, P. D. Battle, J. C. Burley, Daniel J. Gallon, Clare P. Grey, S. H. Kim, J. Mater. Chem. **10**, 2612 (2003).
 - ¹⁷ K. M. Mogare, K. Friese, W. Klein, and M. Jansen, Z. Anorg. Allg. Chem. **630**, 547 (2004).
 - ¹⁸ J. Darriet and J. Galy, Bull. Soc. fr. Mineral. Cristallogr. **97**, 3 (1974).
 - ¹⁹ We believe there are two typographical errors in the table of atomic coordinates in Ref. 10. The z fractional coordinate of site Na₃ and the y fractional coordinate of site O₃ should each be approximately 0.5.
 - ²⁰ M. Drillon, J. Darriet, and R. Georges, J. Phys. Chem. Solids **38**, 411 (1977).
 - ²¹ T. C. Gibb, R. Greatrex, N. N. Greenwood, J. Solid State Chem. **31**, 153 (1980).
 - ²² K. Kambe, J. Phys. Soc. Jpn. **5**, 48 (1950)
 - ²³ G.L.Squires, *Introduction to the Theory of Thermal Neutron Scattering* (Dover, 1996).
 - ²⁴ J.T. Haraldsen, T. Barnes, and J. L. Musfeldt, Phys. Rev. B **71**, 064403 (2005).
 - ²⁵ N. G. Parkinson, P. D. Hatton, J. A. K. Howard, C. Ritter, F. Z. Chiend and M.-K Wue, J. Mater. Chem **13**, 1468 (2003).
 - ²⁶ N. G. Parkinson, P. D. Hatton, J. A. K. Howard, S. R. Giblin, I. Terry, C. Ritter, B.-H. Mokd and M.-K. Wud, J. Mater. Chem **15**, 1375 (2005).
 - ²⁷ M. Arai, A.D. Taylor, S.M. Bennington, and Z.A. Bowden, in *Recent Developments in the Physics of Fluids*, W.S. Howells & A.K. Soper eds, p. F291 (Adam Hilger, Bristol, 1992).
 - ²⁸ C.J. Carlile and M.A. Adams, Physica B **182**, 431 (1992).
 - ²⁹ N. W. Ashcroft and N. D. Mermin, *Solid State Physics* (Thomson Learning, 1976).